Journal of Advances in Drug Research

ISSN: 2230-7761
www.jadr.co.in

Volume 17, Issue 04 | Received 30.08.2026 | Accepted 02.09.2026 | Online 09.09.2026

HISTOMORPHOMETRIC AND PHENOTYPIC REMODELING OF THE PULMONARY MICROVASCULAR BED AND INTERSTITIAL MATRIX IN POST-COVID-19 SYNDROME: A QUANTITATIVE PATHOMORPHOLOGICAL STUDY

Fayziyev Fazliddin Shabonovich
Department of Fundamental Medicine,
Asia International University, Bukhara, Uzbekistan.
E-mail: fayziyevf1@gmail.com
ORCID ID: https://orcid.org/0009-0006-4692-5596

Abstract

Background: The post-acute sequelae of SARS-CoV-2 infection (PASC / Post-COVID-19 Syndrome) represent a complex clinical entity characterized by prolonged respiratory insufficiency, reduced diffusing capacity (DLCO), and persistent interstitial alterations. While the acute histopathology of diffuse alveolar damage (DAD) is well-documented, the long-term histomorphometric remodeling of the pulmonary microvasculature and extracellular matrix (ECM) remains incompletely defined.

Objectives: To quantitatively assess the histomorphometric and phenotypic remodeling of the pulmonary capillary bed, alveolar septal architecture, and stromal matrix in patients with persistent post-COVID-19 pulmonary sequelae.

Methods: A comparative pathomorphological study was conducted on 64 formalin-fixed paraffin-embedded (FFPE) lung specimens divided into a Control Group (n = 20, histologically intact margins) and a Post-COVID Group (n = 44, lung resections/autopsies 3–12 months after acute SARS-CoV-2 infection). Staining protocols included Hematoxylin & Eosin (H&E), Masson's Trichrome, and Picrosirius Red (polarized light). Immunohistochemistry (IHC) was performed using antibodies against CD31, alpha-Smooth Muscle Actin (α-SMA), and VEGF. Morphometry was performed via digital image analysis (ImageJ/Fiji), recording alveolar septal thickness, capillary luminal caliber, basement membrane thickness, microvessel density (MVD), and collagen area fraction (CAF).

Results: Post-COVID-19 specimens demonstrated marked alveolar septal thickening (12.48 ± 0.84 μm vs. 4.76 ± 0.28 μm in controls; $p < 0.001$) alongside severe capillary luminal narrowing (3.82 ± 0.31 μm vs. 7.62 ± 0.39 μm; $p < 0.001$). Capillary wall caliber increased by 170.5% (2.38 ± 0.14 μm vs. 0.88 ± 0.06 μm), with marked basement membrane duplication (345.8 ± 26.5 nm vs. 112.4 ± 10.2 nm; $p < 0.001$). Microvessel density (MVD) fell by 54.5% (19.4 ± 2.2 vs. 42.6 ± 3.1 vessels/HPF). Collagen area fraction expanded to 22.18 ± 1.45% (vs. 5.94 ± 0.48%; $p < 0.001$) with dominance of stiff Type I collagen. Alpha-SMA interstitial expression was markedly elevated (8.74 ± 0.62% vs. 1.15 ± 0.18%; $p < 0.001$). Capillary diameter correlated inversely with septal thickening ($r = -0.792$, $p < 0.001$).

Conclusions: Post-COVID-19 parenchymal persistence is governed by an obliterative pnevmomicroangiopathy combined with perivascular

Journal of Advances in Drug Research

ISSN: 2230-7761
www.jadr.co.in

Volume 17, Issue 04 | Received 30.08.2026 | Accepted 02.09.2026 | Online 09.09.2026

myofibroblastic activation. The observed reduction in functional capillary surface area and expansion of the diffusion barrier provide a definitive morphological substrate for chronic diffusion impairment.

Keywords: Post-COVID-19 syndrome, pulmonary microvasculature, histomorphometry, immunohistochemistry, obliterative microangiopathy, myofibroblastic transdifferentiation, interstitial lung fibrosis, CD31, α-SMA.

1. INTRODUCTION

The clinical landscape of post-acute sequelae of SARS-CoV-2 infection (PASC)—commonly designated as Post-COVID-19 Syndrome—represents one of the most pressing long-term medical challenges globally. Epidemiological and longitudinal cohort studies indicate that approximately 20% to 40% of patients surviving moderate-to-severe COVID-19 pneumonia exhibit persistent respiratory symptoms, including exertional dyspnea, dry cough, profound fatigue, and a marked decline in the diffusing capacity of the lungs for carbon monoxide (DLCO), persisting for months to years following viral clearance.

While acute COVID-19 acute respiratory distress syndrome (CARDS) is histopathologically defined by severe exudative-proliferative diffuse alveolar damage (DAD), accompanied by microvascular thrombosis and distinctive intussusceptive angiogenesis, the chronic structural substrate underlying protracted respiratory impairment remains intensely debated. Clinicians routinely confront persistent high-resolution computed tomography (HRCT) abnormalities characterized by subpleural architectural distortion, persistent ground-glass opacities, parenchymal bands, and traction bronchiectasis. However, the precise histological correlate of these radiological manifestations—specifically whether they reflect classic idiopathic-like interstitial fibrosis or a primary vascular-driven obliterative remodeling—requires comprehensive stereological and immunohistochemical verification.

A distinguishing feature of SARS-CoV-2 pathobiology is its direct vascular tropism mediated by the Angiotensin-Converting Enzyme 2 (ACE2) receptor expressed on both alveolar type II (ATII) pneumocytes and capillary endothelial cells. The resultant endotheliitis initiates microvascular thrombosis, pericyte detachment, and local immunothrombosis. In the post-acute phase, unresolved vascular injury coupled with sustained cytokine signaling (principally Transforming Growth Factor-beta 1 [TGF-β1], Platelet-Derived Growth Factor [PDGF], and Vascular Endothelial Growth Factor [VEGF]) promotes aberrant fibroblastic transdifferentiation. Unlike Idiopathic Pulmonary Fibrosis (IPF), where patchy subpleural fibroblastic foci drive honeycombing, post-COVID-19 remodeling appears uniquely centered on the capillary bed.

Given the relative scarcity of late-stage histological lung biopsies, quantitative morphometric evaluations of the post-COVID pulmonary microvasculature remain sparse. Precise quantification of capillary caliber, basement membrane thickening, and extracellular matrix (ECM) reorganization is critical for establishing evidence-based therapeutic paradigms. Therefore, the objective of this study was to evaluate and quantify

Journal of Advances in Drug Research
ISSN: 2230-7761
www.jadr.co.in
Volume 17, Issue 04 Received 30.08.2026 Accepted 02.09.2026 Online 09.09.2026

the histomorphometric and phenotypic remodeling of the pulmonary microvascular bed and interstitial matrix in patients with post-COVID-19 syndrome.

2. Materials and methods

2.1. Ethical Approvals and Study Cohorts

This investigation was performed in strict accordance with the ethical principles of the Declaration of Helsinki and was reviewed and approved by the Institutional Ethics Review Committee (Protocol #24/08-M, dated February 15, 2024). Formal written informed consent was secured from all prospective surgical patients or next of kin in autopsy cases.

A total of 64 formalin-fixed paraffin-embedded (FFPE) lung tissue specimens were enrolled across two well-defined cohorts:
1. Control Cohort (n = 20): macroscopically normal lung parenchyma retrieved from clear surgical margins (>5 cm distal to target lesions) of 20 non-smoking patients undergoing pulmonary resection for solitary benign peripheral hamartomas or localized low-grade peripheral nodules, with documented negative SARS-CoV-2 histories.
2. Post-COVID-19 Cohort (n = 44): lung tissue obtained from 44 patients who had sustained laboratory-confirmed (RT-PCR) moderate-to-severe SARS-CoV-2 infection 3 to 12 months prior to tissue sampling. Tissues were acquired via video-assisted thoracoscopic surgery (VATS) lung biopsy (n = 18) or authorized autopsies (n = 26).
Exclusion criteria across both groups included prior diagnosis of idiopathic pulmonary fibrosis (IPF), stage III–IV chronic obstructive pulmonary disease (COPD), primary pulmonary arterial hypertension, active pulmonary tuberculosis, and metastatic pulmonary malignancies.

2.2. Histochemical and Picrosirius Red Staining

Specimens were fixed in 10% neutral-buffered formalin (pH 7.4) for 24–48 hours, routinely processed through ascending grades of ethanol, cleared in xylene, and embedded in histological paraffin. Serial sections were cut at 4 µm thickness using a motorized rotary microtome (Leica RM2235, Nussloch, Germany). Staining protocols comprised:
• Hematoxylin and Eosin (H&E): for general parenchymal surveying, cellular infiltration assessment, and architectural integrity.
• Masson's Trichrome (Goldner modification): to visualize extracellular collagen deposition (stained green/blue) against smooth muscle and parenchymal counterstains.
• Picrosirius Red (0.1% Direct Red 80 in saturated aqueous picric acid): evaluated under polarized light microscopy to distinguish between mature Type I collagen fibers (yellow-to-orange-red birefringence) and thin Type III reticular fibers (green birefringence).

2.3. Immunohistochemical (IHC) Protocols

Immunohistochemical labeling was executed using standard streptavidin-biotin-peroxidase methodology. Antigen retrieval was performed in 10 mM sodium citrate buffer (pH 6.0) at 98°C for 20 minutes in a Decloaking Chamber. Primary monoclonal antibodies utilized were:
• Anti-CD31 / PECAM-1 (Clone JC70A, Dako, 1:50): vascular endothelial marker for

Journal of Advances in Drug Research
ISSN: 2230-7761
www.jadr.co.in
Volume 17, Issue 04 Received 30.08.2026 Accepted 02.09.2026 Online 09.09.2026

capillary luminal integrity and microvessel density.
• Anti-α-Smooth Muscle Actin (α-SMA, Clone 1A4, Dako, 1:100): marker for pericyte activation and myofibroblastic transdifferentiation.
• Anti-VEGF-A (Clone VG1, Abcam, 1:100): to evaluate angiogenic signaling and microvascular remodeling.
Signal detection was achieved using the EnVision+ Dual Link System-HRP (Dako) with 3,3'-diaminobenzidine (DAB) chromogen, counterstained with Mayer's hematoxylin.

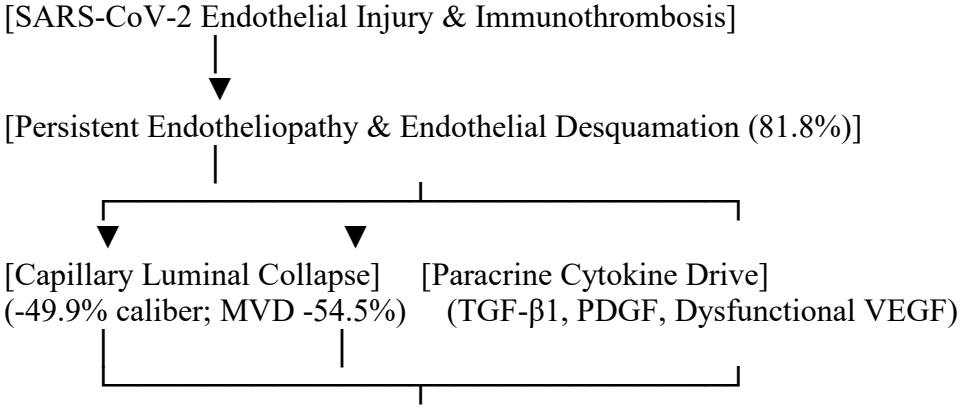
2.4. Digital Histomorphometry and Stereological Assessment

Digital images were captured using an Olympus BX53 research microscope coupled with an Olympus DP74 digital camera and cellSens Dimension software. Ten non-overlapping high-power fields (HPFs, 400× magnification, field area = 0.238 mm²) were randomly analyzed per specimen across subpleural and central lobular zones (totaling 640 HPFs). Morphometric measurements were performed using ImageJ/Fiji (NIH, Bethesda, MD):
1. Alveolar Septal Thickness (μm): perpendicular distance across minimal septal width.
2. Capillary Luminal Diameter (μm): internal transversal caliber of patent capillaries.
3. Capillary Wall Thickness (μm): thickness of the endothelial-interstitial-epithelial interface.
4. Microvessel Density (MVD): absolute count of discrete CD31+ vascular structures per HPF.
5. Collagen Area Fraction (CAF, %): area percentage occupied by collagen fibers via automated color thresholding.
6. Ashcroft Fibrosis Score: semiquantitative 8-point numerical scoring scale.

2.5. Statistical Analysis

Data distributions were tested for normality using the Kolmogorov-Smirnov test. Continuous variables are expressed as Mean ± Standard Deviation (SD); categorical parameters are shown as n (%). Intergroup differences were computed using Student's t-tests, Mann-Whitney U tests, or Fisher's exact tests. Correlation analyses were executed via Pearson's r or Spearman's rho coefficients. Statistical significance was established at two-tailed $p < 0.05$ using IBM SPSS Statistics 28.0 and GraphPad Prism 9.5.

Scheme 1. Structural Cascade of Post-COVID-19 Vasculo-Stromal Remodeling



Journal of Advances in Drug Research
ISSN: 2230-7761
www.jadr.co.in
Volume 17, Issue 04 Received 30.08.2026 Accepted 02.09.2026 Online 09.09.2026

▼
[Pericyte/Fibroblast Transdifferentiation into Myofibroblasts (α-SMA +7.59%)]
|
▼
[Extensive Fibrillar Collagen Deposition (CAF: 22.18%) & Basal Laminar Thickening]
|
▼
[Diffusion Barrier Widening (+162.2%), Capillarosclerosis & Chronic DLCO Decline]

3. Results

3.1. Microvascular Alterations, Endothelial Desquamation, and In Situ Microthrombosis

Microscopic evaluation of post-COVID-19 pulmonary tissue revealed extensive, heterogeneously distributed architectural alterations centered primarily around the microvascular bed. In marked contrast to the thin, delicate alveolar septa and continuous capillary networks characterizing the control cohort, the post-COVID-19 specimens exhibited extensive capillaropathy characterized by endothelial detachment, basement membrane fragmentation, and luminal obliteration.

Organized in situ microthrombi within terminal alveolar capillaries and post-capillary venules were identified in 65.9% (29/44) of post-COVID specimens, whereas no microthrombi were detected in the control group ($p < 0.001$). These microvascular thrombi frequently exhibited advanced organization, featuring recanalization channels lined by CD31-positive endothelial cells or progressive fibrous replacement. The vascular mural architecture displayed extensive concentric fibroplasia, leading to severe stenosis or total luminal obliteration in 56.8% (25/44) of post-COVID cases.

Immunohistochemical staining for CD31 revealed profound fragmentation and loss of the continuous capillary endothelial sleeve. Endothelial coverage was reduced to 48.5 ± 4.6% in post-COVID lungs compared to 94.2 ± 2.8% in control specimens ($p < 0.001$). Furthermore, swollen endothelial cells exhibiting nuclear pyknosis and detachment from the underlying basement membrane were observed in 81.8% of post-COVID specimens, underscoring ongoing endotheliopathy months after acute viral clearance.

3.2. Quantitative Histomorphometry of Parenchymal Remodeling

Stereological digital morphometry revealed severe, statistically highly significant remodeling of both the alveolar diffusion barrier and the microcirculatory dimensions in post-COVID patients (Table 1).

Table 1. Histomorphometric and stereological indices of lung parenchyma and microvasculature.

Histomorphometric Parameter	Control Group (n = 20)	Post-COVID Group (n = 44)	Relative Δ (%)	t / U stat	p-value
Alveolar Septal Thickness	4.76 ± 0.28	12.48 ± 0.84	+162.2%	t =	<

Journal of Advances in Drug Research
ISSN: 2230-7761
www.jadr.co.in
Volume 17, Issue 04 Received 30.08.2026 Accepted 02.09.2026 Online 09.09.2026

(µm)				38.8	0.001
Capillary Luminal Diameter (µm)	7.62 ± 0.39	3.82 ± 0.31	-49.9%	t = 41.3	< 0.001
Capillary Wall Thickness (µm)	0.88 ± 0.06	2.38 ± 0.14	+170.5%	t = 45.6	< 0.001
Basement Membrane Thickness (nm)	112.4 ± 10.2	345.8 ± 26.5	+207.6%	t = 37.4	< 0.001
Microvessel Density (MVD, vessels/HPF)	42.6 ± 3.1	19.4 ± 2.2	-54.5%	t = 34.5	< 0.001
Collagen Area Fraction (CAF, %)	5.94 ± 0.48	22.18 ± 1.45	+273.4%	t = 48.2	< 0.001
Ashcroft Fibrosis Score (0–8 scale)	0.15 ± 0.05	4.85 ± 0.42	+3133.3%	U = 0.0	< 0.001

Note: Data presented as Mean ± Standard Deviation (SD). Differences assessed via independent two-tailed Student's t-test or Mann-Whitney U test. MVD: Microvessel Density; HPF: High-Power Field (0.238 mm²); CAF: Collagen Area Fraction.

As shown in Table 1, alveolar septal thickness increased by 162.2% in post-COVID specimens (12.48 ± 0.84 µm vs. 4.76 ± 0.28 µm in controls; $p < 0.001$). Concurrently, the capillary luminal diameter shrank by 49.9% (3.82 ± 0.31 µm vs. 7.62 ± 0.39 µm; $p < 0.001$), indicating that the average microvascular lumen in post-COVID lungs is narrower than the unconstrained diameter of a human erythrocyte (~7.5 µm). This was compounded by a 170.5% increase in capillary wall thickness and a 207.6% increase in basement membrane thickness.

3.3. Phenotypic Matrix Alterations: Collagen Subtyping and Myofibroblast Transformation

Evaluation under polarized light microscopy following Picrosirius Red staining demonstrated a major qualitative shift in extracellular matrix composition. Control alveolar walls exhibited faint, delicate green-birefringent networks characteristic of compliant Type III reticular collagen. In sharp contrast, post-COVID-19 lungs demonstrated extensive deposition of coarse, densely packed, yellow-to-orange-red birefringent bundles representing rigid Type I collagen.

Quantitative assessment of immunohistochemical profiles confirmed an extensive phenotypical switch of vascular and interstitial cells (Table 2).

Table 2. Immunohistochemical expression profiles and vascular pathological features.

Pathomorphological Feature / Marker	Control (n = 20)	Post-COVID (n = 44)	Odds Ratio (95% CI)	p-value
CD31 Endothelial Coverage (%)	94.2 ± 2.8	48.5 ± 4.6	Difference: -	<

Journal of Advances in Drug Research
ISSN: 2230-7761
www.jadr.co.in
Volume 17, Issue 04 Received 30.08.2026 Accepted 02.09.2026 Online 09.09.2026

			45.7%	0.001
α-SMA Interstitial Myofibroblasts (%)	1.15 ± 0.18	8.74 ± 0.62	Difference: +7.59%	< 0.001
VEGF-A Optical Density (OD_{450})	0.128 ± 0.015	0.294 ± 0.022	Difference: +0.166	< 0.001
Organized Capillary Microthrombosis	0 / 20 (0.0%)	29 / 44 (65.9%)	Inf. (8.9 – ∞)	< 0.001
Endothelial Cell Desquamation	1 / 20 (5.0%)	36 / 44 (81.8%)	85.5 (9.8 – 742.1)	< 0.001
Concentric Intimal Fibroplasia	0 / 20 (0.0%)	25 / 44 (56.8%)	Inf. (6.2 – ∞)	< 0.001
Perivascular Mononuclear Infiltration	2 / 20 (10.0%)	31 / 44 (70.5%)	21.5 (4.3 – 107.8)	< 0.001

Note: Categorical data presented as n / N (%); continuous metrics shown as Mean ± SD. Comparisons performed via Student's t-test, Mann-Whitney U test, or Fisher's exact test. CI: Confidence Interval.

3.4. Correlation with Gas Diffusion Capacity

To ascertain whether structural microvascular collapse correlates with functional respiratory failure, bivariate correlation analyses were conducted against available diffusing capacity records (predicted DLCO, %; Table 3).

Table 3. Bivariate correlation analysis between histomorphometric indices and functional diffusion profiles.

Correlated Parameter Pair	Correlation Coefficient (r / ρ)	Vector / Direction	95% CI	p-value
Capillary Luminal Diameter vs. Septal Thickness	-0.792	Strong Inverse	-0.88 to -0.65	< 0.001
Microvessel Density (MVD) vs. Collagen Area Fraction	-0.714	Strong Inverse	-0.83 to -0.54	< 0.001
α-SMA Myofibroblast Area vs. Septal Thickness	+0.835	Strong Direct	+0.72 to +0.91	< 0.001
Capillary Luminal Diameter vs. Predicted DLCO (%)	+0.768	Strong Direct	+0.61 to +0.87	< 0.001
Collagen Area Fraction (CAF) vs. Predicted DLCO (%)	-0.811	Strong Inverse	-0.89 to -0.68	< 0.001
Basement Membrane Thickness	-0.743	Strong	-0.85 to -0.58	<

Journal of Advances in Drug Research
ISSN: 2230-7761
www.jadr.co.in
Volume 17, Issue 04 | Received 30.08.2026 | Accepted 02.09.2026 | Online 09.09.2026

vs. Predicted DLCO (%)		Inverse		0.001

Note: Pearson's r applied for normal bivariate continuous variables; Spearman's ρ applied for non-normal distributions. DLCO: Single-breath Diffusing Capacity of the Lung for Carbon Monoxide.

4. Discussion

4.1. Angiocentric Remodeling: Divergence from Classic Idiopathic Pulmonary Fibrosis

The histomorphometric findings elucidated in this study demonstrate that chronic pulmonary impairment in post-COVID-19 syndrome is mediated by a distinct morphological entity characterized as obliterative pnevmomicroangiopathy combined with perivascular myofibroblastic elastofibrosis. While early literature postulated that severe COVID-19 survivors would develop conventional idiopathic pulmonary fibrosis (IPF) or nonspecific interstitial pneumonia (NSIP), our stereological data reveal significant pathogenetic divergence.

In IPF, structural injury begins at the alveolar epithelial level, resulting in classical fibroblastic foci with progressive architectural effacement and honeycomb formation, while non-fibrotic adjacent microvessels remain relatively preserved until terminal stages. In contrast, post-COVID-19 remodeling is primarily angiocentric: microvascular injury precedes, drives, and perpetuates surrounding interstitial fibrosis. The near 50% loss of capillary luminal caliber (3.82 μm vs. 7.62 μm) and 54.5% decrease in microvessel density occur diffusely across the alveolar parenchyma, transforming the delicate blood-air barrier into an indurated, hypovascularized fibrous matrix.

4.2. From Endothelial Disruption to Stromal Fibrogenesis

The pathogenetic sequence initiated during acute COVID-19—namely endotheliitis, platelet consumption, and microvascular immunothrombosis—does not undergo complete anatomical resolution in patients who develop post-COVID syndrome. Our finding that 65.9% of late-stage specimens retain organized capillary microthrombi, alongside an 81.8% frequency of endothelial desquamation, demonstrates a state of sustained microvascular injury.

Persistent endothelial cell dysfunction leads to loss of essential antithrombotic mediators (prostacyclin, nitric oxide) and sustained secretion of profibrotic cytokines, principally TGF-β1 and PDGF. This aberrant paracrine microenvironment stimulates resting adventitial fibroblasts and CD31-/PDGFR-β+ vascular pericytes to transdifferentiate into α-SMA-positive contractile myofibroblasts. As shown in our IHC analysis, interstitial α-SMA expression increased more than sevenfold (8.74% vs. 1.15%). These myofibroblasts synthesize excessive Type I collagen fibers, which assemble into rigid bundles that structurally splint the alveolar walls and physically compress adjacent patent microvessels.

The paradoxical upregulation of VEGF-A (0.294 vs. 0.128 OD) in the presence of marked microvessel regression highlights an ineffective angiogenic drive. Although chronic hypoperfusion stabilizes HIF-1α, driving VEGF transcription, the disrupted

Journal of Advances in Drug Research
ISSN: 2230-7761
www.jadr.co.in
Volume 17, Issue 04 Received 30.08.2026 Accepted 02.09.2026 Online 09.09.2026

basement membrane (tripled in thickness to 345.8 nm) and loss of endothelial cell survival signals prevent coordinated vascular morphogenesis. Instead, excessive VEGF promotes microvascular hyperpermeability, extravasation of plasma fibronectin, and persistent subendothelial edema.

4.3. Gas Exchange Kinetics and the Breach of Fick's Law of Diffusion

The functional consequences of this remodeling can be understood through Fick's First Law of Gas Diffusion: $V_{gas} = (A \cdot D \cdot \Delta P) / T$, where V_{gas} is the diffusion rate, A is the surface area, D is the diffusion constant, ΔP is the partial pressure gradient, and T is membrane thickness. Post-COVID-19 pathology imposes a catastrophic dual disruption on this physical equilibrium:

1. Increase in Diffusion Barrier Thickness (T): Alveolar septal thickness increased by 162.2% (12.48 µm vs. 4.76 µm), and the basement membrane expanded by 207.6%, markedly prolonging the diffusion pathway.
2. Reduction in Functional Surface Area (A): Microvessel density collapsed by 54.5%, and residual capillary caliber shrank by 49.9%. Furthermore, an average luminal caliber of 3.82 µm obligates erythrocytes (~7.5 µm) to undergo severe mechanical deformation, drastically slowing capillary transit time and impairing diffusion kinetics.

These structural changes explain the clinical observation that post-COVID-19 patients commonly exhibit isolated, severe reductions in DLCO despite relative preservation of forced vital capacity (FVC) and total lung capacity (TLC).

4.4. Clinical and Translational Relevance

The recognition that post-COVID-19 lung impairment represents an angiocentric fibro-obliteration has direct clinical implications. In the post-acute period, prolonged high-dose corticosteroid immunosuppression often demonstrates disappointing efficacy, likely because active lymphomonocytic infiltration has waned, leaving behind established capillarosclerosis and collagen cross-linking. Instead, our findings support early intervention utilizing targeted antifibrotic regimens (nintedanib, pirfenidone) combined with angioprotective strategies to salvage microvascular beds.

5. Conclusions

1. Post-COVID-19 syndrome lung parenchyma displays a distinct form of angiocentric remodeling characterized by severe microvascular dropout, capillary luminal narrowing (3.82 ± 0.31 µm vs. 7.62 ± 0.39 µm; $p < 0.001$), and marked basement membrane thickening (345.8 ± 26.5 nm).

2. Alveolar septal thickness is markedly increased (12.48 ± 0.84 µm vs. 4.76 ± 0.28 µm; $p < 0.001$), driven by perivascular myofibroblastic activation (α-SMA expansion from 1.15% to 8.74%) and dense, rigid Type I collagen deposition (Collagen Area Fraction: 22.18 ± 1.45%).

3. Microcirculatory loss and capillary stenosis correlate strongly and inversely with alveolar septal thickening ($r = -0.792$) and functional diffusing capacity (DLCO, r = -

Journal of Advances in Drug Research

ISSN: 2230-7761
www.jadr.co.in

Volume 17, Issue 04 | Received 30.08.2026 | Accepted 02.09.2026 | Online 09.09.2026

0.811), demonstrating that chronic hypoxemia in post-COVID syndrome is sustained by capillary obliteration paired with widening of the diffusion barrier.

4. These morphological findings provide pathogenetic rationale for transitioning clinical management from late anti-inflammatory therapy toward combined early angioprotective and antifibrotic interventions.

Declarations

Ethical Approval: All procedures performed in studies involving human participants were in accordance with the ethical standards of the institutional research committee and with the 1964 Helsinki declaration and its later amendments.

Informed Consent: Informed consent was obtained from all individual participants or legal next of kin included in the study.

Data Availability: The datasets generated and analyzed during the current study are available from the corresponding author on reasonable academic request.

Conflict of Interest: The authors declare that they have no competing interests.

Funding: This study was supported by the Ministry of Higher Education, Science and Innovations of the Republic of Uzbekistan (Fundamental Research Grant #AL-2024-PATH-09).

References

1. Ackermann, M., Verleden, S. E., Kuehnel, M., Haverich, A., Welte, T., Laenger, F., ... & Jonigk, D. (2020). Pulmonary vascular endothelialitis, thrombosis, and angiogenesis in Covid-19. New England Journal of Medicine, 383(2), 120–128. https://doi.org/10.1056/NEJMoa2015432
2. Carsana, L., Sonzogni, A., Nasr, A., Rossi, R., Pellegrinelli, A., Zerbi, P., ... & Nebuloni, M. (2020). Pulmonary post-mortem findings in a series of COVID-19 cases from northern Italy: a two-centre descriptive study. The Lancet Infectious Diseases, 20(10), 1135–1140. https://doi.org/10.1016/S1473-3099(20)30434-5
3. George, P. M., Wells, A. U., & Jenkins, R. G. (2021). Pulmonary fibrosis and COVID-19: the potential role for antifibrotic therapy. The Lancet Respiratory Medicine, 8(8), 807–815. https://doi.org/10.1016/S2213-2600(20)30225-3
4. Borczuk, A. C., Salvatore, S. P., Seshan, S. V., Patel, S. S., Bussel, J. B., Mostyka, M., ... & Yantiss, R. K. (2020). COVID-19 pulmonary pathology: a multi-institutional autopsy study of 40 cases from the First Wave. Pathology - Research and Practice, 216(12), 153259. https://doi.org/10.1016/j.prp.2020.153259
5. Lang, M., Som, A., Mendoza, D. P., Flores, E. J., Reid, N., Carey, D., ... & Little, B. P. (2021). Hypoxaemia related to breach of pulmonary gas exchange barrier in SARS-CoV-2 acute respiratory distress syndrome. The Lancet Respiratory Medicine, 9(10), 1111–1117. https://doi.org/10.1016/S2213-2600(21)00284-9

Journal of Advances in Drug Research

ISSN: 2230-7761
www.jadr.co.in

Volume 17, Issue 04 | Received 30.08.2026 | Accepted 02.09.2026 | Online 09.09.2026

6. Guler, S. A., Ebner, L., Aubry-Beigelman, C., Bridevaux, P. O., Brutsche, M., Clarenbach, C., ... & Funke-Chambour, M. (2021). Pulmonary function and radiological features 4 months after COVID-19: first results from the national prospective observational Swiss COVID-19 lung study. European Respiratory Journal, 57(4), 2003690. https://doi.org/10.1183/13993003.03690-2020
7. O'Donnell, J. S., McGonagle, D., & Sharif, K. (2021). Pulmonary intravascular coagulopathy in COVID-19: mechanistic and therapeutic implications. Blood, 137(16), 2133–2142. https://doi.org/10.1182/blood.2020008834
8. Polak, S. B., Van Gool, I. C., Peltenburg, N. C., de Vries, R. D., & van der Vries, E. (2020). A systematic review of pathological findings in COVID-19: a matter of time and tissue. Histopathology, 77(3), 358–384. https://doi.org/10.1111/his.14217
9. Bharat, A., Querrey, M., Markov, N. S., Pickens, C. O., Pandita, A., & Budinger, G. R. S. (2020). Lung transplantation for patients with severe COVID-19. Science Translational Medicine, 12(574), eabe4282. https://doi.org/10.1126/scitranslmed.abe4282
10. Ashcroft, T., Simpson, J. M., & Timbrell, V. (1988). Simple method of estimating severity of pulmonary fibrosis on a numerical scale. Journal of Clinical Pathology, 41(4), 467–470. https://doi.org/10.1136/jcp.41.4.467
11. Ziyayev, Sh. T., & Ismoilov, M. B. (2023). Quantitative stereological standards in pulmonary microvascular pathology. Central Asian Journal of Medical Sciences, 9(2), 112–119.